NASA TECHNICAL NOTE

NASA TN D-2782

NASA TN D-2782

BACKSCATTERING AND SECONDARY-ELECTRON EMISSION FROM METAL TARGETS OF VARIOUS THICKNESSES

by Allan J. Cohen and Kenneth F. Koral

Lewis Research Center
Cleveland, Ohio

NATIONAL AERONAUTICS AND SPACE ADMINISTRATION • WASHINGTON, D. C. • APRIL 1965

NASA TN D-2782

BACKSCATTERING AND SECONDARY-ELECTRON EMISSION FROM METAL TARGETS OF VARIOUS THICKNESSES

By Allan J. Cohen and Kenneth F. Koral

Lewis Research Center
Cleveland, Ohio

NATIONAL AERONAUTICS AND SPACE ADMINISTRATION

For sale by the Clearinghouse for Federal Scientific and Technical Information
Springfield, Virginia 22151 – Price $2.00

BACKSCATTERING AND SECONDARY-ELECTRON EMISSION FROM METAL TARGETS OF VARIOUS THICKNESSES

by Allan J. Cohen and Kenneth F. Koral

Lewis Research Center

SUMMARY

Measurements were made of the number of backscattered and secondary electrons resulting from the impingement of primary electrons in the energy range 0.6 to 1.8 MeV upon thin targets of seven metals. The materials ranged from aluminum, with an atomic number of 13, to gold, with an atomic number of 79. Included in the investigation were the effects upon backscattering and secondary-electron coefficients of changes in both primary-electron energy and angle of incidence, as well as target thickness and atomic number. It was determined that a thickness equivalent to, or greater than, one-half range acts as an infinite backscatterer. Also, it was found that an energy-independent correlation of backscattering yield with thickness exists for each metal target. A linear increase in the secondary-electron coefficient with the backscattering coefficient was observed. Backscattering coefficients were measured as low as 0.4 percent and as high as 62 percent, and secondary-electron yields ranged from 1.1 to 5.2 percent.

INTRODUCTION

The beta radioisotope cell, which has been proposed as a lightweight electric powerplant (ref. 1), has a beta source deposited on a metal foil and enclosed inside a thin metal collector. Backdirected electrons (both backscattered and secondary electrons) arising from the impingement of beta particles (energetic electrons) on metal surfaces will detract from the performance of the cell. Published data on the backdirected electron phenomenon are very scanty in the energy range of a disintegrating beta emitter. It was the purpose of this study to obtain information on the amount of backscattered and secondary electrons produced by metal targets so that the effects of these phenomena can be minimized in the design of the radioisotope cell. This report presents the basic data obtained. Empirical formulas for representing the backscattering data and application of the results to the radioisotope cell are the subjects of a current investigation.

When an incident beam of highly energetic electrons strikes a metal target, a complicated set of physical phenomena is initiated. The electrons penetrate the metal and lose energy, roughly in proportion to path length in the metal. Some of these electrons are deflected as they approach the nuclei of the metal atoms by an amount predicted from the Rutherford scattering formula. Also, some of the surface electrons of the target material are energized by the

passing primary electrons. As a result of these encounters, electrons will reemerge from the metal on the entrance side of the foil. These backdirected electrons belong to two groups. One group is composed of primary electrons that have been turned around and are referred to as backscattered electrons. The other group are secondary electrons ejected from the surface of the target metal by acquiring energy from the incoming primary electrons. The backscattered electrons are observed (ref. 2) to have a continuous energy spectrum ranging from the incident energy of the primary electrons down to near zero energy, where the yield becomes negligibly small. The secondary electrons also have a continuous energy spectrum, but it ranges from zero electron volts to about 50 electron volts, above which the number of secondaries becomes negligibly small (ref. 2). Because the number of backscattered electrons below 50 electron volts is negligible (ref. 3), these two groups of electrons can be separated by their different range of energies.

In the impinging electron energy range of this study (0.6 to 1.8 MeV), some measurements on the production of backscattered and secondary electrons have been made previously. The number of backscattered electrons per primary beam electron has been measured for many thick, impenetrable targets in the energy range 1.0 to 3.0 MeV (ref. 4). Similar information has been presented for the energy range below 0.3 MeV (ref. 5). Also, measurements exist for secondary electrons in the range of interest for three materials of very thin foils that stop or deflect only a small fraction of incident electrons (ref. 6). Besides these measurements, angular distributions of backscattered electrons from incident electrons at 1.75 MeV upon penetrable targets have been obtained (ref. 7). These data, however, are not sufficient for estimating the magnitude of the problem for isotope power generation of the type proposed in reference 1.

In the present investigation, information on the backscattering yield from primary electrons with energies from 0.6 to 1.8 MeV has been obtained for targets ranging in thickness from very thin to impenetrable for seven metals. Additional measurements are presented for secondary-electron emission from these targets with the effect of backscattering included. Measurements have also been made to ascertain the effect on backscattering and secondary-electron coefficients of a change in the angle of incidence of the primary electrons. Angles of 30°, 45°, and 60° are considered in addition to normal incidence.

The phenomenon of backscattering in the experiment is complicated not only by the continuous loss of energy suffered by the incident electrons but also by the numerous collisions which can occur before an electron reemerges from the material. For these reasons, and because of the mathematical complexity of the Rutherford scattering function, there exists no satisfactory theory for multiple backscattering. In the case of the production of secondary electrons, however, a satisfactory semiempirical theory does exist (refs. 2 and 6). In the backscattering portion of the report, measurements are evaluated and plotted with two new variables, target thickness and angle of incidence, incorporated into the study. The effect of these variables has not been previously reported. In the secondary-electron portion of the study, older techniques are applied to a higher energy range than has previously been investigated, with clear and interesting results.

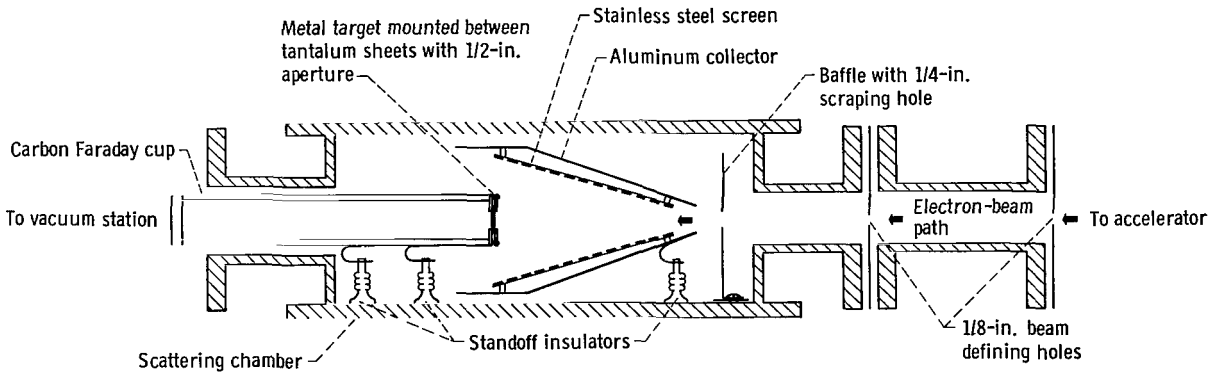

(a) Arrangement for normal-incidence measurement.

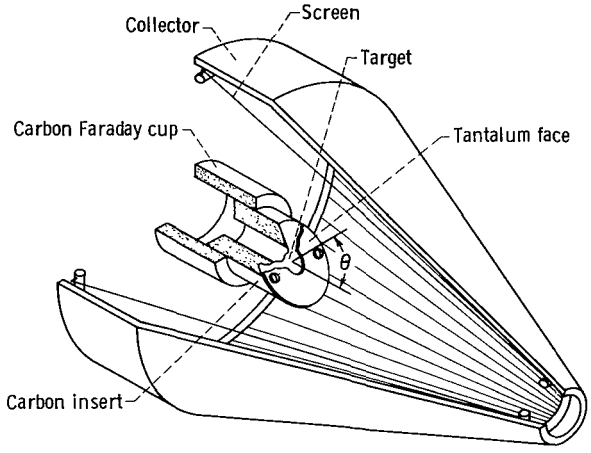

(b) Details of angular insert to experimental apparatus for modification to angular measurement.

Figure 1. - Apparatus for backscattering experiment.

The present investigation was conducted with the 3-MeV Dynamitron (ref. 8) at the Lewis Research Center.

APPARATUS

The experimental apparatus was designed to measure backscatter and secondary-electron production from metal targets. Figure 1(a) is a layout of the mechanical apparatus used. A slightly divergent electron beam from the accelerator first passes through a collimator before entering the experimental region. The collimator consists of two 1/8-inch-diameter holes to define the beam and a 1/4-inch scraping hole to divest the beam of the halo of deflected electrons. All three holes are drilled in thin but impenetrable tantalum sheets so that slit-edge scattering might be minimized. The baffle with the scraping hole in it protects the experiment from stray electrons entering from

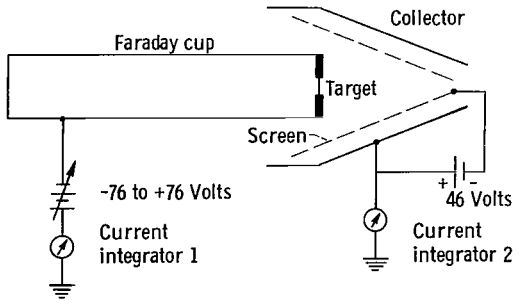

Figure 2. - Electrical diagram for backscattering experiment.

the collimator region. Before the experiment can take place these holes must be properly alined. The well-defined beam from the collimator is directed toward a carbon Faraday cup upon which are mounted the thin metal targets. An aperture on the front of the Faraday cup is 1/2 inch in diameter. The aperture, which is completely covered by the targets, was cut from two pieces of tantalum (10 and 15 mils thick), the total thickness of which is capable of stopping the maximum-energy electrons used in the experiment. Targets are set between these two pieces of tantalum, which are then fastened to the front of the Faraday cup. The carbon Faraday cup has a 2-inch inside diameter and is 2 feet long. A conical aluminum collector surrounds the front of the Faraday cup and the mounted target. The cone is 1/8 inch thick and covers the entire backscattering hemisphere except for a small beam opening. This thickness of aluminum is capable of stopping the maximum-energy electrons used in the experiment. A conical screen grid is located between the target and the collector mounted 1/4 to 1/2 inch away from the collector surface. The purpose of the grid is to suppress secondary electrons from the collector. The grid wires cover 10 percent of the area of the collector as seen by the backdirected electrons. The entire experiment is set inside a scattering chamber, which is evacuated to a pressure of approximately 4×10^{-5} torr during the experimental runs.

The same experimental apparatus can be used for angles other than normal incidence by modifying the carbon Faraday cup as shown in figure 1(b). Cylindrical carbon inserts faced off at different angles to the cylindrical axis are placed in the carbon Faraday cup. The inserts have two pieces of tantalum foil covering their front openings with elliptical apertures cut from them. The targets are placed between the two pieces of tantalum in the same manner as for the normal-incidence setup.

Figure 2 is a schematic of the electrical circuit used in the experiment. The measurements are obtained from current integrators that are suited to the fluctuating currents obtained from the electron accelerator. The integrators measure total charge, and this can be equated to current flow when ratios are considered. The screen and collector are connected to integrator 2, and the Faraday cup and target are connected to integrator 1. The screen is biased to -46 volts with respect to the collector to return the secondary electrons ejected from the collector surface. The collector is grounded (through integrator 2) so that any stray secondaries in the scattering chamber that have been introduced from the collimating region will not be attracted to the collector and thereby affect the measurement. The electrical bias needed between the collector and the combination of Faraday cup and target is obtained by setting the electrical potential of the Faraday cup and target above or below ground as required. This bias, as well as the screen bias, is obtained from batteries insulated from ground, and the current flow takes place in shielded cables, which eliminate the effect of noise on the experiment.

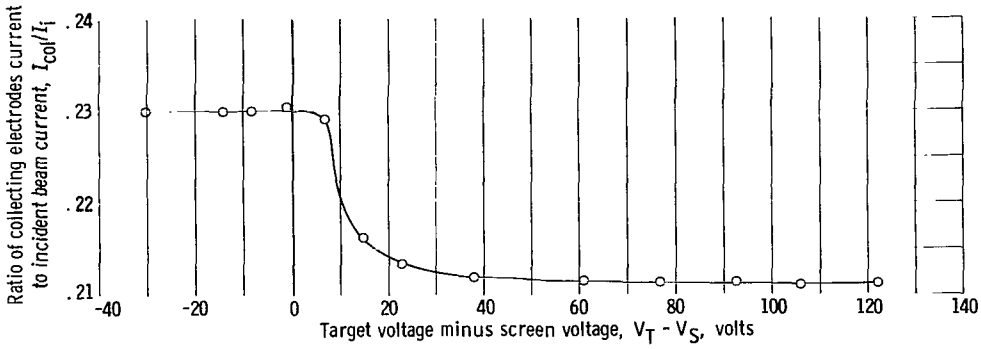

Figure 3. - Relative collecting electrodes current as function of target minus screen voltage.

PROCEDURE

Method

As stated in the preceding section, secondary electrons emitted by a foil under electron bombardment have energies less than about 50 electron volts. The technique in the present experiment was to measure first all backdirected electrons from the bombarded target foil, and then, by preventing secondary electrons from being collected, to measure only the backscattered electrons. The total number of backdirected electrons minus the number of backscattered electrons equals the number of secondary electrons.

The two measurements are obtained with the target and Faraday-cup potential set 76 volts above and below ground. The experimental results of continuously varying this voltage are shown in figure 3, which is a plot of the ratio of current to the collector and screen to incident beam current I_{col}/I_i against the voltage difference $V_T - V_S$ (target voltage minus screen voltage). (All symbols are defined in appendix A.) When $V_T - V_S$ is negative, backscattered and secondary electrons are being collected. As this voltage difference increases, the current drops, since the secondary electrons are attracted back to the target and prevented from reaching the collecting electrodes. The plateau regions of figure 3 are very flat, and it can be seen that the energy of secondary electrons (between the plateau regions) is limited to about 30 electron volts.

Measurements

The customary method of expressing the magnitude of backscattering or secondary emission is as a yield or coefficient, defined as the ratio of the number of electrons undergoing the given process divided by the total number of incident electrons. In the experiment, the backscattering yield η is determined from

$$\eta = \frac{I_{col}^{+}}{I_i} \tag{1}$$

where I^+_{col} is the current to the collecting electrodes with $V_T - V_S = 122$ volts and I_i is the incident beam current.

The secondary yield can be obtained by subtracting the backscattered yield from the total backdirected yield. The secondary-electron yield δ is therefore given by the expression

$$\delta = \Delta - \eta \tag{2}$$

with

$$\Delta = \frac{I^-_{col}}{I_i} \tag{3}$$

where Δ is the total backdirected electron yield and I^-_{col} is the current to the collecting electrodes with $V_T - V_S = -30$ volts.

From figure 2, the current to the collecting electrodes is measured by current integrator 2. The total current from the target and Faraday cup I_F is measured by current integrator 1. Regardless of the voltage setting, the total beam current, after striking the target, flows to ground through meters 1 and 2 so that

$$I_i = I_F + I^+_{col} \tag{4a}$$

or

$$I_i = I_F + I^-_{col} \tag{4b}$$

When equations (4) are used, equations (1) and (3) become

$$\eta = \frac{I^+_{col}}{I_F + I^+_{col}} \tag{5}$$

$$\Delta = \frac{I^-_{col}}{I_F + I^-_{col}} \tag{6}$$

Since the time of integration is the same for all currents for a given measurement, the counterparts of equations (5) and (6) in terms of charge are exactly equivalent.

During the experiment, both the current to the collecting electrodes and that to the target and Faraday cup were simultaneously integrated over a period of 1 to several minutes. The incident current I_i had a value between 1×10^{-6} and 4×10^{-6} ampere. The magnitude of the current to the collecting electrodes I_{col} depended on the target and the incident current and ranged from 0.9×10^{-8} to 1.9×10^{-6} ampere. The currents I_{col} and I_F were measured twice for each data point to check primary energy drift.

The energy of the accelerator is determined by measuring the current through a calibrated resistor. Reproducibility of a given energy is good to about 0.1 percent. The absolute accuracy of the energy is, according to a scintillation crystal pulse height analysis, 4 percent at energies up through 1.4 MeV and 5 percent and 8 percent at 1.6 and 1.8 MeV, respectively. These errors were not random in nature, but were in the form of energy setting inaccuracies.

Targets

Target materials were aluminum, iron, nickel, molybdenum, silver, tantalum, and gold, so that the range of Z was from 13 to 79. Most of the target foils were about 1 square inch in area and between 0.001 and 0.010 inch in thickness. The range of the product of density and target thickness t was 12.7 to 494 milligrams per square centimeter.

The foils were 99 percent pure metal and had surfaces without visual defects. They were cleaned with acetone and then with alcohol before being put into the scattering chamber.

Sources of Errors

Escape of electrons. - The beam entrance hole in the aluminum collector subtends a solid angle to the target of about 0.019 steradian and permits a loss of some emitted electrons. At normal incidence for thick targets the backscattered electrons can be assumed to follow a cosine distribution (ref. 7), and the measured backscattering yields can be 0.6 percent too low because of this loss. The secondary yields are not affected because of the collector bias. For thinner targets and angular incidences the backscattering distributions are not as concentrated in the beam hole direction. In all cases, therefore, the error is small and can be neglected.

Backscattering from the collecting electrodes and secondaries from the screen. - Backscattering of electrons from the collecting electrodes with the eventual loss of these electrons from the measurement causes a decrease in the observed values of the backscattering yield. The magnitude of this decrease for normal incidence cannot be calculated exactly, but it is estimated in appendix B as about 5 percent. This represents the most significant error in the backscattering yields and means that the absolute values of these yields for normal incidence are accurate to within about 5 percent.

During the backscattering measurement, secondary electrons emitted from the screen return to the target. This causes the observed values of the backscattering coefficients to be low and those of the secondary coefficient to be high. It is estimated that the ratio of the return current of secondaries from the collecting electrodes with a screen-collector bias to that without a bias is equal to the ratio of the cross-sectional area of the screen to the area of the collector. When this estimate is applied to a measurement of a thick nickel target at normal incidence, the error in the backscattering yield is

0.6 percent, which is negligible, and the error in the secondary yield is 5 percent. Therefore, in general, the absolute accuracies of the experimental secondary-emission coefficients are also limited to about 5 percent.

Faraday cup and slit-edge scattering. - Backscatter out of the Faraday cup and collimator slit-edge scatter to the collector are sources of error that increase the values of the backscattering yields. The Faraday-cup backscattered current consists of electrons which penetrate the target foil, backscatter off of one or more Faraday-cup surfaces, and have sufficient energy to pass through the target foil. The 2-foot length and carbon composition of the Faraday cup and the small target area were all designed to minimize this error.

The amount of these errors was measured without a target in place. Over the entire energy range, the total stray current was less than 0.06 percent of the incident beam current. It was estimated from geometrical considerations that the contribution to the error with a target in place is not significantly greater than the small value without a target.

Accelerator variations. - Reproducibility checks on the measured backscattering coefficients show some variations that are due to the difficulty of reproducing experimental conditions. Two values differ by, in general, less than ±0.3 percent for thick targets and less than 2 percent for the thin targets. For the secondary coefficients it is estimated that energy drift and other accelerator variations cause value variations of less than ±5 percent for all targets.

When a complete total of the errors is made, the backscattering coefficients are accurate within +7 percent and -2 percent, and secondary-emission values have accuracies of +5 percent and -10 percent.

RESULTS AND DISCUSSION

Backscattering

Theory. - When a highly energetic electron passes near the nucleus of an atom, it is deflected (scattered) by the coulomb forces exhibited by the two interacting bodies. The cross section σ for the scattering of an electron of rest energy m_0c^2 beyond an angle θ' by a nucleus of charge Ze, is predicted by the Rutherford scattering equation (ref. 9, p. 592)

$$\sigma = \pi\left(\frac{Ze}{m_0c^2}\right)^2 \frac{1}{\left(E' - \frac{1}{E'}\right)^2} \cot^2 \frac{\theta'}{2} \tag{7}$$

where E' is the total energy $(E + m_0c^2)$ of the passing electron in units of m_0c^2 (0.511 MeV). The equation, while not including electron screening or quantum-mechanical effects, correctly indicates the large effects of the atomic number Z, the primary-electron kinetic energy E, and the scattering angle θ' upon the single scattering process of the electron-nucleus encounter. In the targets tested the primary electrons are scattered many times before they re-

emerge from the metal. This multiple scattering process requires a statistical evaluation of the Rutherford cross section, a theoretical problem which at present has no satisfactory solution. However, since the backscattering measured in the experiment is multiple coulomb scattering, some of the trends in the backscattering coefficient due to a change in energy, atomic number, and angle of incidence may agree approximately with equation (7) (ref. 10).

In addition to the plurality of deflections, the impinging electrons suffer an energy loss, primarily to the electrons of the target. This energy loss tends to mask further the simple Rutherford description of the coulomb scattering phenomenon.

A further result of primary-electron energy loss in the present experiment can be illustrated as follows: If a primary electron, on penetrating a target, loses all of its initial energy, it will stop and be absorbed in the material. The maximum distance an energetic electron can travel in a material before losing its energy is called its range. (Straggling is neglected in this report.) A good formula for the range of an electron R in aluminum is the Katz and Penfold relation (ref. 11), valid in the range 0.1 MeV < E < 2.5 MeV:

$$R = 412E^{(1.265-0.0954 \ln E)} \text{ mg/sq cm} \qquad (8)$$

which was empirically fit to experimental data. It can be applied to other metals by the insertion of the factor $\frac{A}{Z}\frac{13}{27}$ on the right side of equation (8) (ref. 12). If an electron of energy E strikes a target of thickness t equal to one-half of the electron range (with straggling neglected), the electron will have just enough energy to traverse the metal completely and, if properly directed, still be a backscattered electron. Thus, a thickness equal to or greater than one-half range is equivalent to an arbitrarily large thickness with regard to backscattering. In the present study, the value of the energy corresponding to the half-range thickness is evaluated for many of the targets. Also, curves of backscattering against thickness, presented in the section backscattering as function of thickness, will show the saturation effect of the half-range thickness upon the backscattering phenomenon.

Backscattering as function of energy. - Backscattering coefficients (eq. (5)) were evaluated for each of the targets tested and are recorded in table I (p. 32). These results are also shown in figure 4, where the backscattering coefficient η is plotted as a function of primary energy E for normal incidence. For each of the metals used, curves of η as a function of E are given for several target thicknesses. In all the curves presented, an increase in the primary-electron energy is accompanied by a decrease in the backscattering coefficient. The thickness of the target relative to the energy of the incoming electrons influences the rate with which the decrease occurs and thus determines the general shape of the curves of figure 4. Table II (p. 33) gives the fraction of half-range of each target thickness (calculated from eq. (8)) at each of the measured energies and is a good measure of the relative thickness of the metal targets.

In the region of energy corresponding to infinite thickness (determined

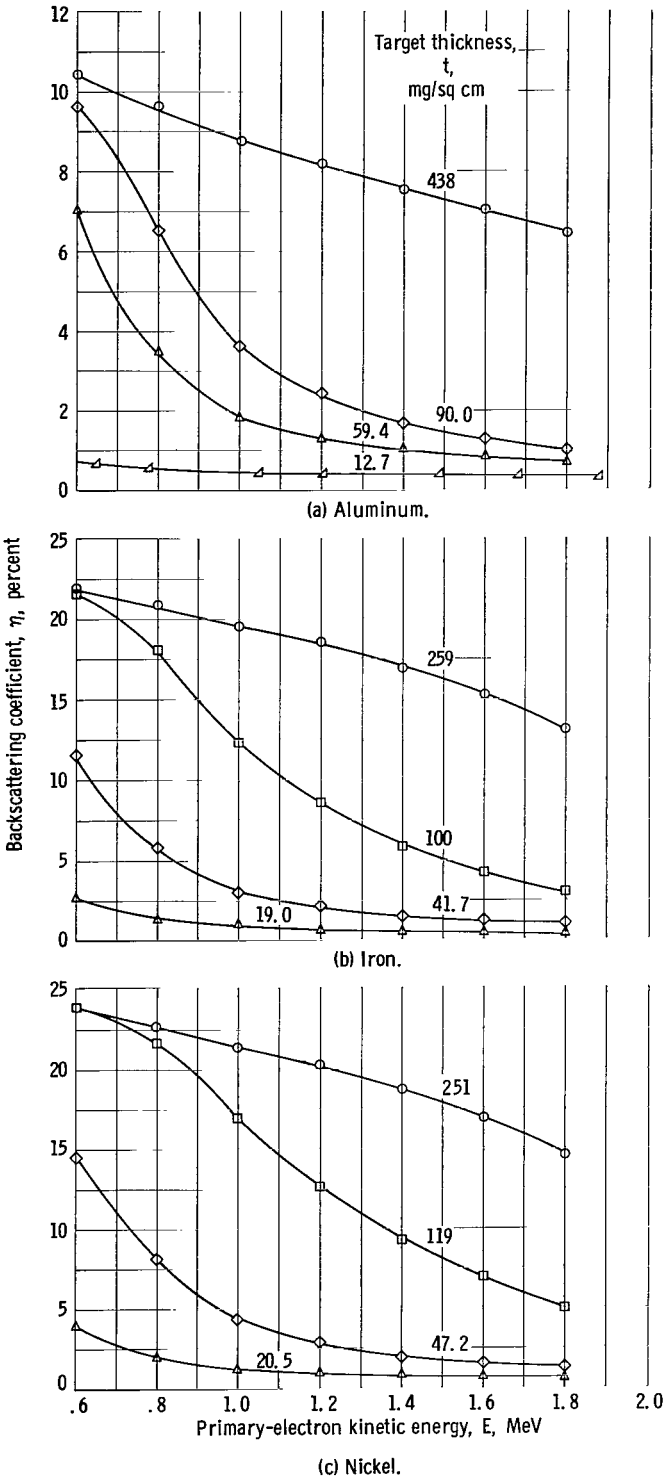

Figure 4. - Backscattering coefficient as function of primary-electron kinetic energy for normal incidence for various target materials.

from table II (p. 33) as equal to or greater than 1.0), the pertinent curves of figure 4 show a very slow decline with a small, almost constant slope. The curves in this region differ from straight lines by a small amount, which becomes negligible for high Z. The value of the backscattering coefficient for the infinite-thickness region will be denoted by η_{max}. When the relative thickness of the targets becomes less than one half-range, (e.g., fig. 4(d), t = 150 mg/sq cm) a change from the slow decline to a more rapid decline occurs (see also table II (p. 33)). These changes can be best seen when two of the upper curves form a single curve in the infinitely thick region and then separate into two curves with increasing energy (e.g., the two upper curves of fig. 4(d)). In the following table, a comparison is made between these separating energies (from fig. 4) and a calculated value of half-range energy. The calculated value is obtained from the Katz-Penfold relation (eq. (8)). The agreement between the calculated values and the graphically determined values is within 10 percent.

As noted previously, for energies greater than the energy corresponding to half-range, the backscattering coefficient decreases rapidly with increasing energy and approaches (for the thinnest targets) a relatively low constant value. The fast-changing region of yield is primarily due to the effect of energy on the coulomb scattering, as predicted in equation (7). The rather slow decline in the region of thickness greater than half-range results from two cancelling effects. One is an increased primary penetration with

Target metal	Target thickness, t, mg/sq cm	Calculated half-range energy, MeV	Graphical energy from curves, MeV
Nickel	119	0.65	0.65
Molybdenum	150	0.73	0.78
	254	1.10	1.15
Silver	128	0.64	0.70
Tantalum	129	0.61	0.68
	187	.80	.86
Gold	242	1.0	1.1

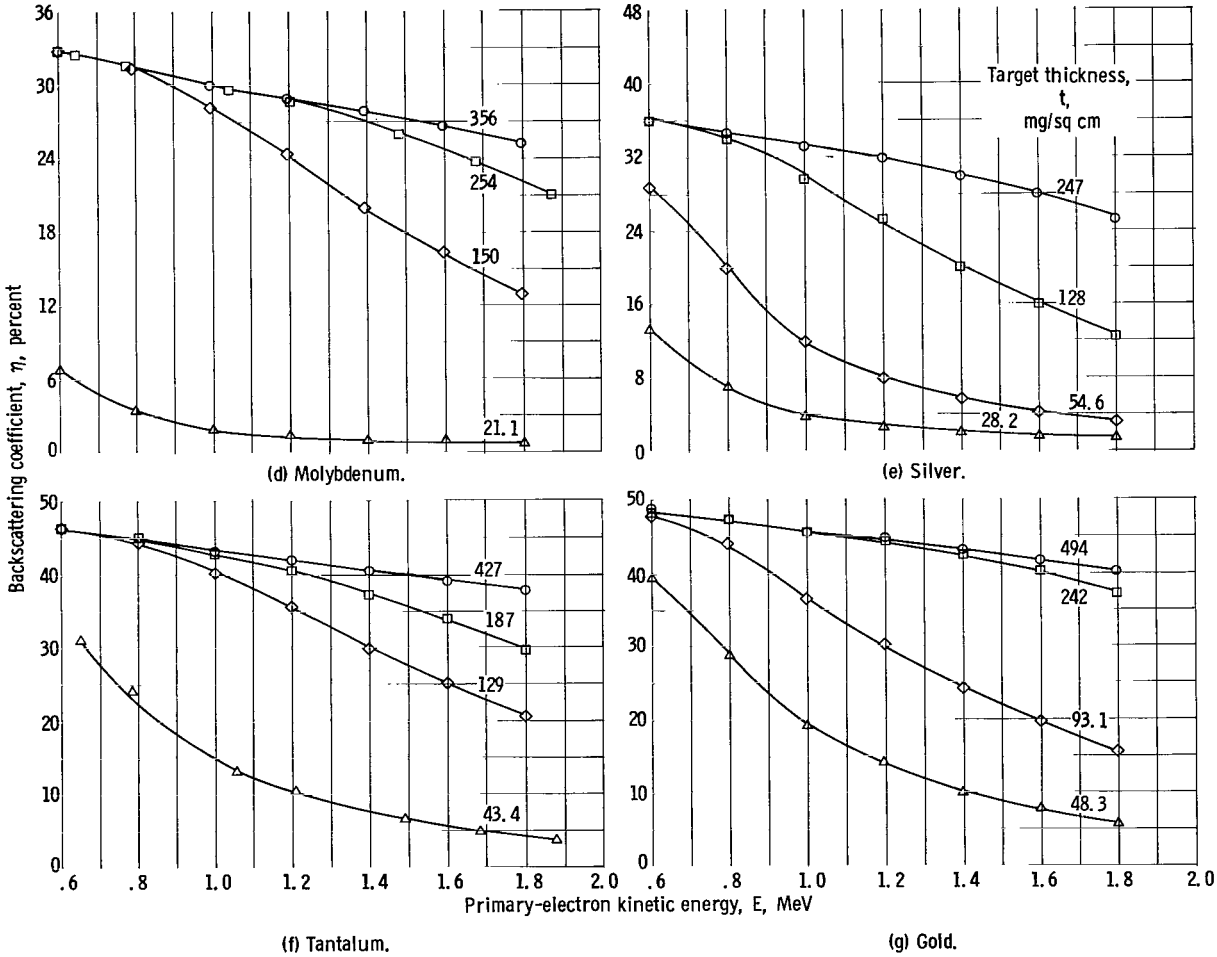

(d) Molybdenum.

(e) Silver.

(f) Tantalum.

(g) Gold.

Figure 4. - Concluded. Backscattering coefficient as function of primary-electron kinetic energy for normal incidence for various target materials.

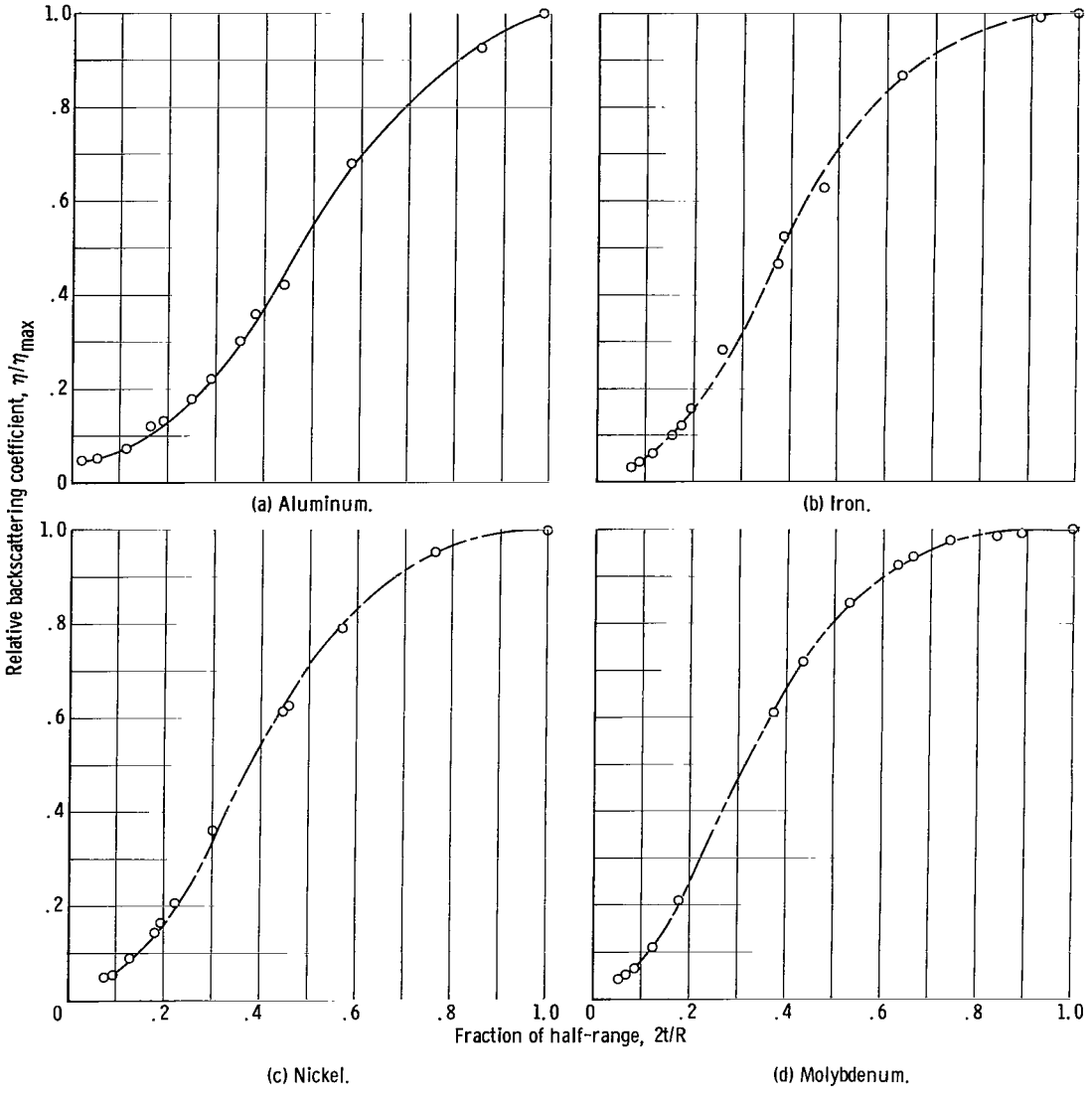

Figure 5. - Relative backscattering coefficient as function of fraction of half-range for normal incidence for various target materials.

increasing energy, which tends to increase η, and the other a decrease in coulomb scattering (eq. (7)), which decreases η. For thin targets only one of these effects remains, that of coulomb scattering. The coulomb scattering alone results in the rapid decline of the backscattering coefficient and probably also in the asymtotic approach to zero at high energies that is apparent in curves for thin samples in figure 4.

Backscattering as function of thickness. - From table I, backscattering could be plotted against target thickness, with energy as a parameter. It was found, though, that for each metal, a single curve, independent of energy, could be produced by using the relative thickness $2t/R$ obtained from table II as the independent variable and a relative backscattering coefficient η/η_{max} as the dependant variable, where η_{max} is the value of the backscattering co-

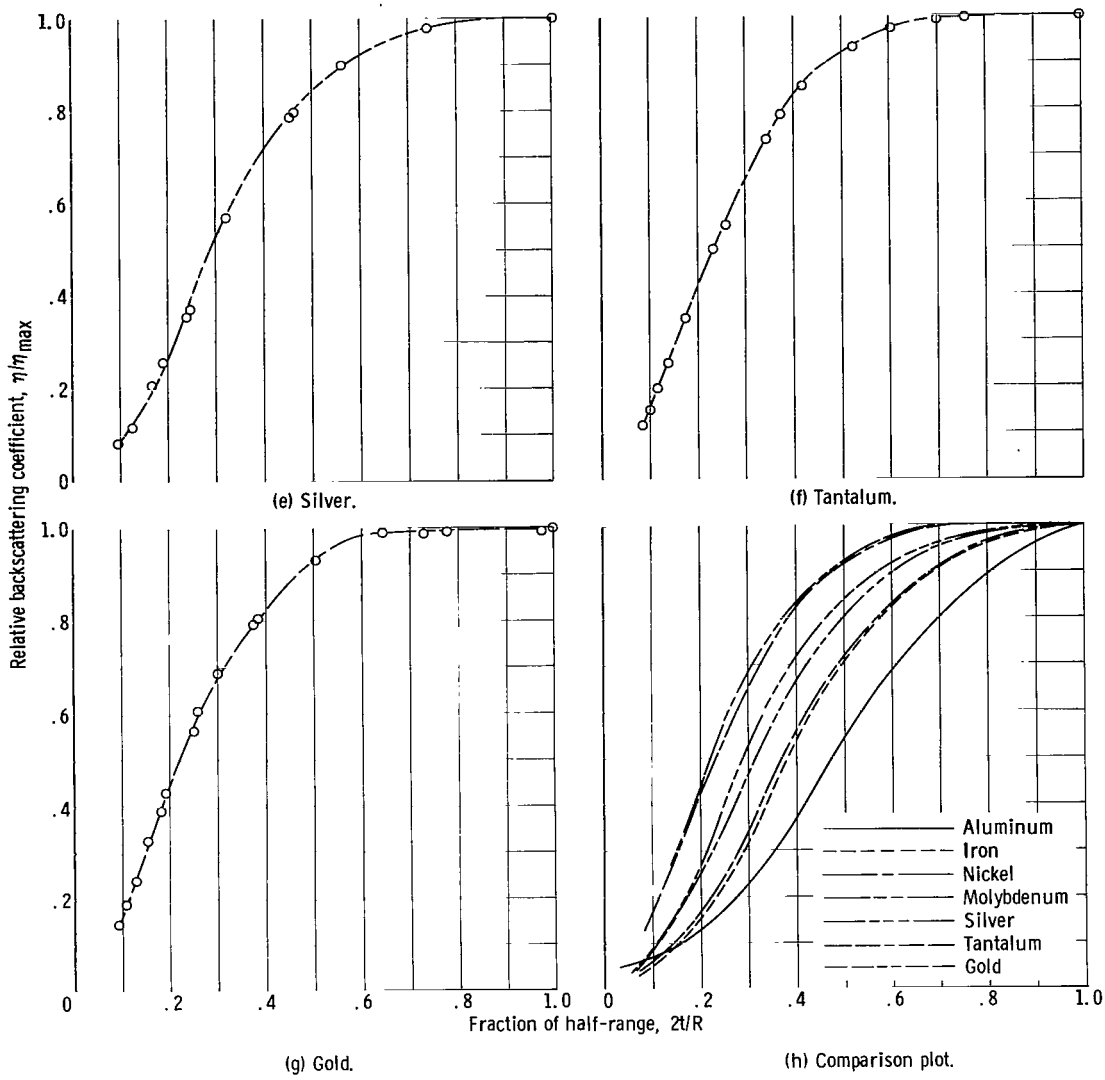

Figure 5. - Concluded. Relative backscattering coefficient as function of fraction of half-range for normal incidence for various target materials.

efficient for infinite thickness. These curves, one for each metal, are shown in figures 5(a) to (g). Figure 5(h) is a comparison of these seven curves. This comparison shows that the relative backscattering ratio approaches its saturation value of unity at lower values of relative thickness as the atomic number of the target increases. The curves pass through the point 1,1 (as they must) and appear in most cases to approach zero at zero relative thickness.

The curves of figure 5 are interesting in that the primary-electron energy enters only in the determination of R and η_{max}. The curves shown represent all the data in the experiment, and it appears probable that they hold true over a much larger energy range. They therefore constitute a correlation, not previously reported, of backscattering against thickness for normal incidence in the kilovolt and low megavolt range of energies.

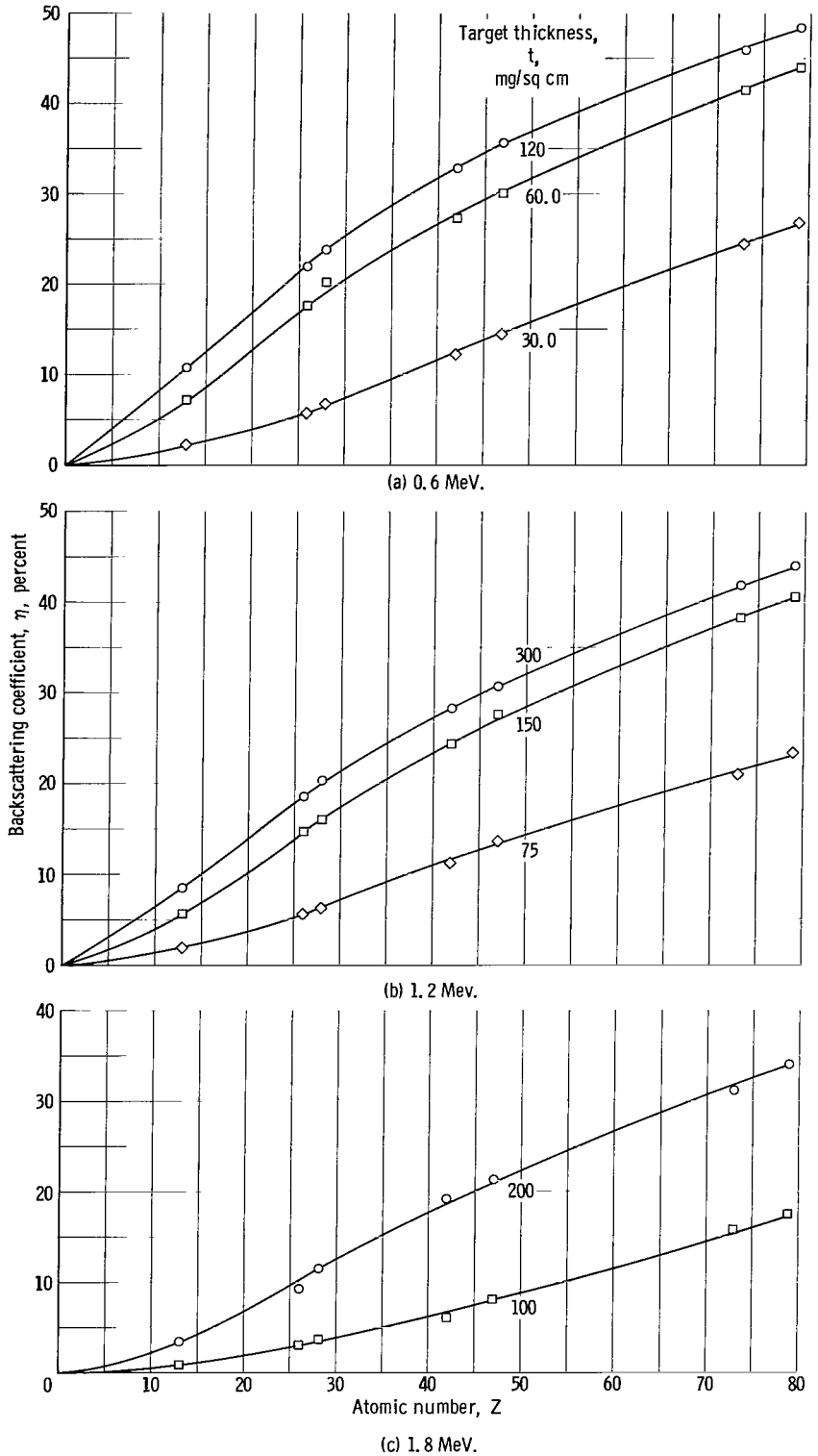

Figure 6. - Backscattering coefficient as function of atomic number for normal incidence for primary-electron kinetic energies of 0.6, 1.2, and 1.8 MeV.

Backscattering as function of atomic number. - The effect of the atomic number of a scattering nucleus on a passing charged particle is large, as is seen in the Rutherford scattering equation (eq. (7)). The effect of the atomic number of the metal targets on the multiple backscattering measured in the present experiment is shown in figure 6 which shows cross plots of figure 5. (Similar curves are presented in ref. 4.) The backscattering coefficient is plotted against atomic number for a few thicknesses and primary-electron energies of 0.6, 1.2, and 1.8 MeV. In the 1.8-MeV plots (fig. 6(c)), a few of the η_{max} values must be obtained through extrapolation of the curves of figure 4. In none of the curves is there any indication of a Z^2 trend as predicted by the Rutherford scattering formula (eq. (7)). However, such agreement should probably not be expected since the energy loss of the primary electrons is not included in the derivation of equation (7).

Backscattering as function of angle of incidence. - The effect of primary-

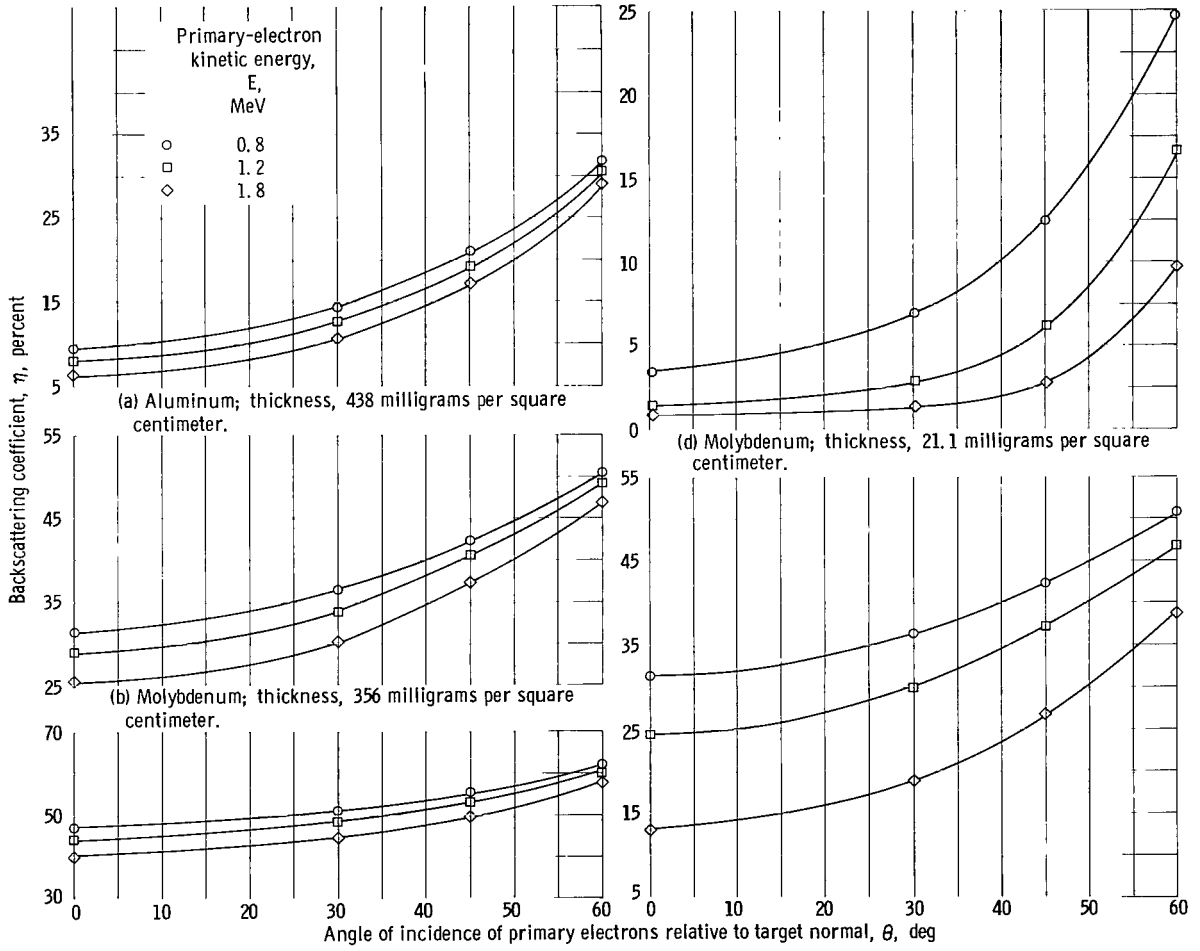

Figure 7. - Backscattering coefficient as function of angle of incidence of primary electrons for aluminum, molybdenum, and gold targets.

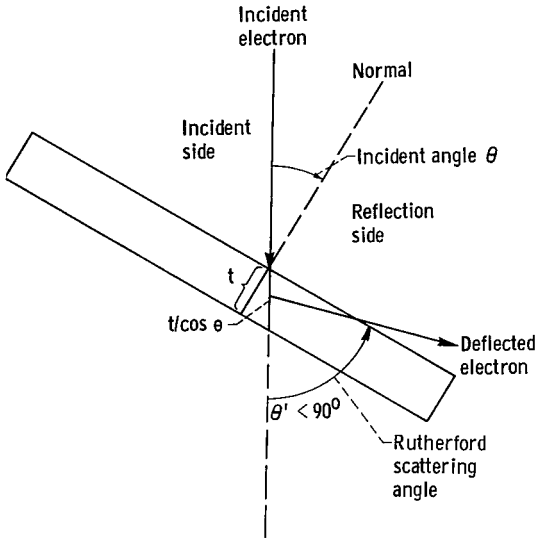

Figure 8. - Diagram for backscattering at angular incidence.

electron incidence angle upon the backscattering coefficient was determined for energies of 0.8, 1.2, and 1.8 MeV. Five different targets were used. Three targets had thicknesses greater than half-range and were made of aluminum, molybdenum, and gold. Two thin molybdenum targets (21.1 and 150 mg/sq cm thick) were also used.

The resulting backscattering ratios are shown in figure 7. For all materials, there is an increase in backscattering with an increase in angle. At high angles of incidence all materials have high backscattering coefficients.

Although the shape of the backscattering coefficient curves seems quite uncomplicated, it does have some interesting features. There is no indication of a leveling off of the curves with increased angle. The increase is probably the result of two effects. First, electrons can be scattered at angles involving deflections of less than 90° on the reflection side (see fig. 8) of the surface of the bombarded targets. According to the Rutherford equation (eq. (7)), this increases the scattering probability, and, according to reference 7, the bulk of the backscattered electrons come out from the target on the reflection side, which is thus the direction of importance. Second, a change from normal incidence increases the effective thickness by providing more path length for backscattering along the straight-through path. In addition, these scattered electrons are closer to the surface by a factor of the cos θ (fig. 8). As a result of these factors an increase in θ produces a favorable condition for backscattering for both thick and thin targets.

A second feature of the experimental results is indicated in the following table, where ratios of the backscattering coefficient at 60° to that at 0° are given for the targets used. These results indicate that the small atomic numbers and the thin targets produce the greatest ratios.

It might be expected that, if the increased straight-line path $t/\cos \theta$ becomes greater than one-half range, the target might behave as an infinite backscatterer even if it is less than one half-range thick. It can be shown from a geometric argument, however, that this is not the case. With oblique incidence, even if the straight-through path is equal to half-range, some of the scattered electrons can escape through the sample in the forward direction. Consequently, a small increase in thickness can increase the backscattering, which is not the case for normal incidence on targets thicker than half-range. This effect can be shown in the experimental data with a comparison of the thick molybdenum curve (fig. 7(b)) and the curve representing 150-milligram-per-square-centimeter molybdenum (fig. 7(e)) at 60° and at 1.2 MeV. Even though at this angle the 150-milligram-per-square-centimeter molybdenum target

Target metal	Atomic number	Target thickness, t, mg/sq cm	Primary-electron kinetic energy, E, MeV	Ratio of backscattering at 60° to that at 0°
Aluminum	13	438	0.8	3.3
			1.2	3.8
			1.8	4.5
Molybdenum	42	356	0.8	1.7
			1.2	1.7
			1.8	1.9
Gold	79	494	0.8	1.3
			1.2	1.3
			1.8	1.4
[a]Molybdenum	42	21.1	0.8	7.3
			1.2	11.8
			1.8	10.9
[a]Molybdenum	42	150	0.8	1.6
			1.2	1.9
			1.8	3.0

[a]Thin targets.

has a straight-through distance of 300 milligrams per square centimeter (> R/2), it does not produce a backscattering ratio as high as the thick molybdenum target.

Secondary Emission

Theory. - Although an exact theory for the complicated process of secondary emission does not exist, there are semiempirical formulas available in the literature. These formulas assume that the secondary-emission yield is proportional to the energy loss of the incident electrons (ref. 2). For bombardment by high-energy electrons

$$\delta_P = \frac{1}{\epsilon} y \frac{dE}{dx} \sec \theta \tag{9}$$

where δ_P is the secondary-electron coefficient due to primaries along, ϵ is a secondary-electron constant characteristic of the material, y is the effective secondary-electron production depth, dE/dx is the rate of energy loss of the incident electrons, and θ is the angle of incidence of primary electrons relative to the target normal (ref. 6).

An expression for the energy loss per unit path length of relativistic electrons based on the work of Bethe and Bloch is (ref. 9, p. 582)

$$\frac{dE}{dx} = \frac{2\pi e^4}{m_o v^2} NZ\left\{\ln\left[\frac{m_o v^2 E}{I^2\left(1 - \frac{v^2}{c^2}\right)}\right] - \frac{v^2}{c^2}\right\} \tag{10}$$

where m_o is the electron rest mass, v is the particle velocity, N is the number of atoms per unit volume in the stopping material, I = (11±3) Z ev, and c is the velocity of light.

Equation (9) does not take into account the fact that backscattered electrons pass through the secondary production region near the surface and thereby excite additional secondary electrons and increase the value of the total secondary-electron yield δ. A formula originated by Dobretsov and Matskevich (ref. 13) predicts the value of the total secondary yield by assuming that it increases linearly with the backscattering yield. The total secondary yield then is

$$\delta = \delta_p + \delta_p^o \beta \eta \tag{11}$$

where δ_p^o is δ_p evaluated at $\theta = 0$, and β is the efficiency of the backscattered electrons for forming secondary electrons.

All the targets of this experiment can be assumed to be much thicker than the depth from which secondary electrons escape (the y of eq. (9)). This depth has been measured to be of the order of tens of Angstroms at keV energies (ref. 14) and should not be significantly greater in the present experiment.

Secondary emission as function of energy. - In figure 9 the experimental values for total secondary-electron yield at normal incidence are plotted against the energy of the primary electrons for each thickness and each material. The values of the secondary coefficient range from 1.1 percent for 21.1-milligram-per-square-centimeter molybdenum at 1.8 MeV (fig. 9(d)) to 3.6 percent for 427-milligram-per-square-centimeter tantalum at 0.6 MeV (fig. 9(f)). The data scatter is slightly greater for the secondary-electron coefficient δ than for the backscattering yield η.

For the thinnest aluminum target in this experiment, the total secondary yield and the yield of secondaries due to primaries are very nearly equal since the backscattering is less than 1 percent. In figure 10, the theoretical curve of the yield of secondaries due to primaries (calculated from eqs. (9) and (10)) is compared with the measured points, and good agreement is obtained. (The y/ϵ of eq. (9) was chosen to match the experimental data at one energy in calculating the curve.) Equations (9) and (10) had been verified previously (ref. 6) for nickel as well as aluminum.

For targets with significant backscattering, the curves of the total secondary-electron yield are composites of the two terms of equation (11). When the backscattering coefficient is small, the first, nearly constant term dominates the dependence on energy, but, when the backscattering coefficient is large, the second term is the dominant one. For all targets, the total

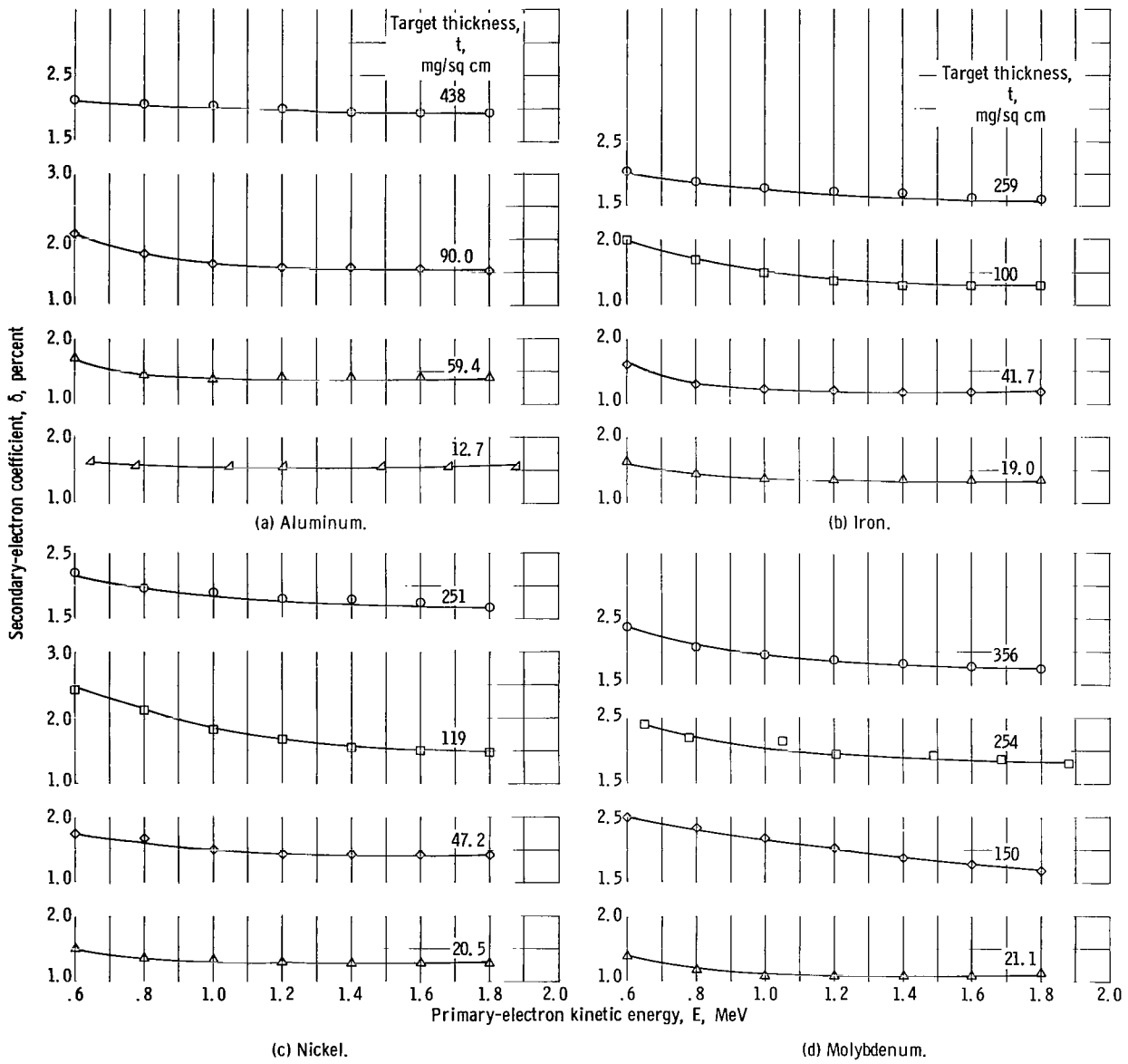

Figure 9. - Secondary-electron coefficient as function of primary-electron kinetic energy for normal incidence for various target materials.

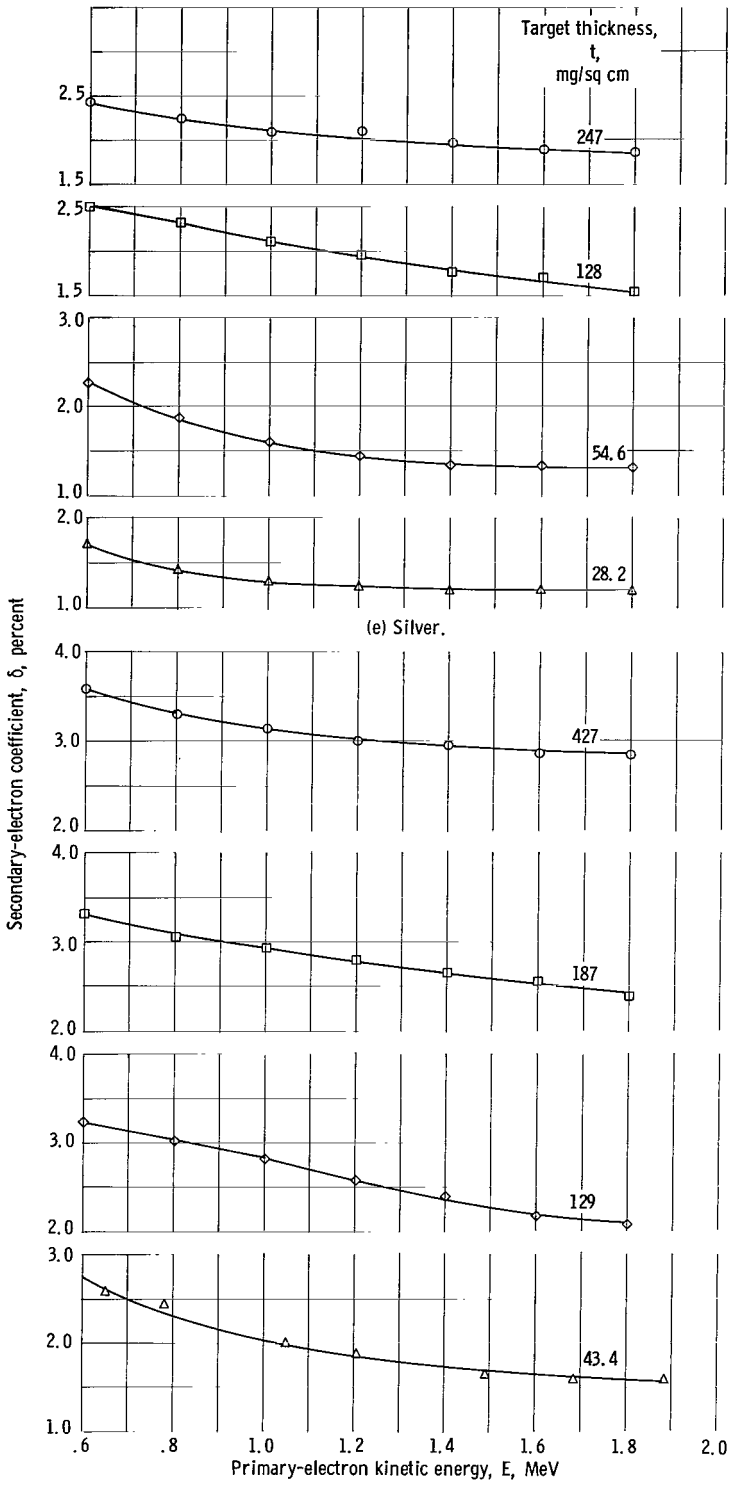

Figure 9. - Continued. Secondary-electron coefficient as function of primary-electron kinetic energy for normal incidence for various target materials.

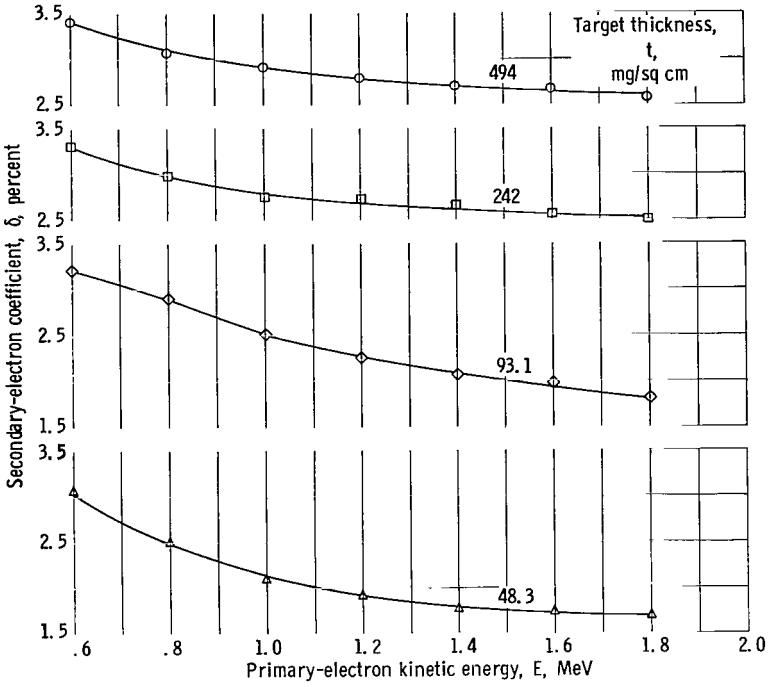

(g) Gold.

Figure 9. - Concluded. Secondary-electron coefficient as function of primary-electron kinetic energy for normal incidence for various target materials.

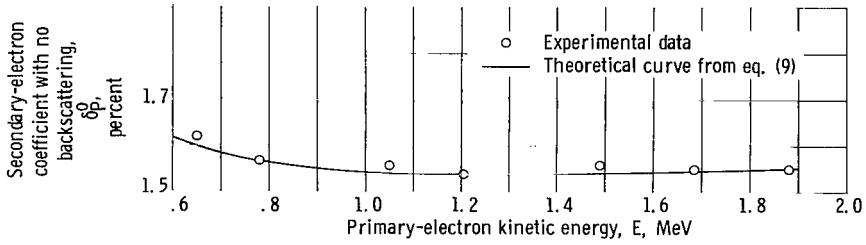

Figure 10. - Comparison of theoretical curve and experimental data. Secondary-electron coefficient due to primaries as function of primary-electron kinetic energy for normal incidence on 12.7 milligrams per square centimeter aluminum target.

secondary yield rises as the energy is reduced.

Surface effects. - It is known that the absolute values of the secondary yields depend on the condition of the surface of the metal. Variations in the coating of oxides or other compounds or other factors make determinations of absolute yields difficult (refs. 2, 6, and 14).

In the present experiment, variations in surface conditions between different targets of the same metal also caused noticeable differences in yield. The magnitude of these differences can be seen by comparing the total secondary yields for different targets of the same material at energies for which the backscattering is the same. These values are collected in the following table.

Target metal	Primary-electron kinetic energy, E, MeV	Target 1	Target 2
		Secondary-electron coefficient, δ, percent	
Nickel	0.6	2.2	2.4
Molybdenum	.6	2.4	2.5
Silver	.6	2.4	2.5
Tantalum	.6	3.6	3.2
Tantalum	.6	3.6	3.3
Tantalum	.8	3.3	3.1
Gold	.6	3.4	3.3
Gold	.8	3.1	3.0
Gold	1.0	2.9	2.8

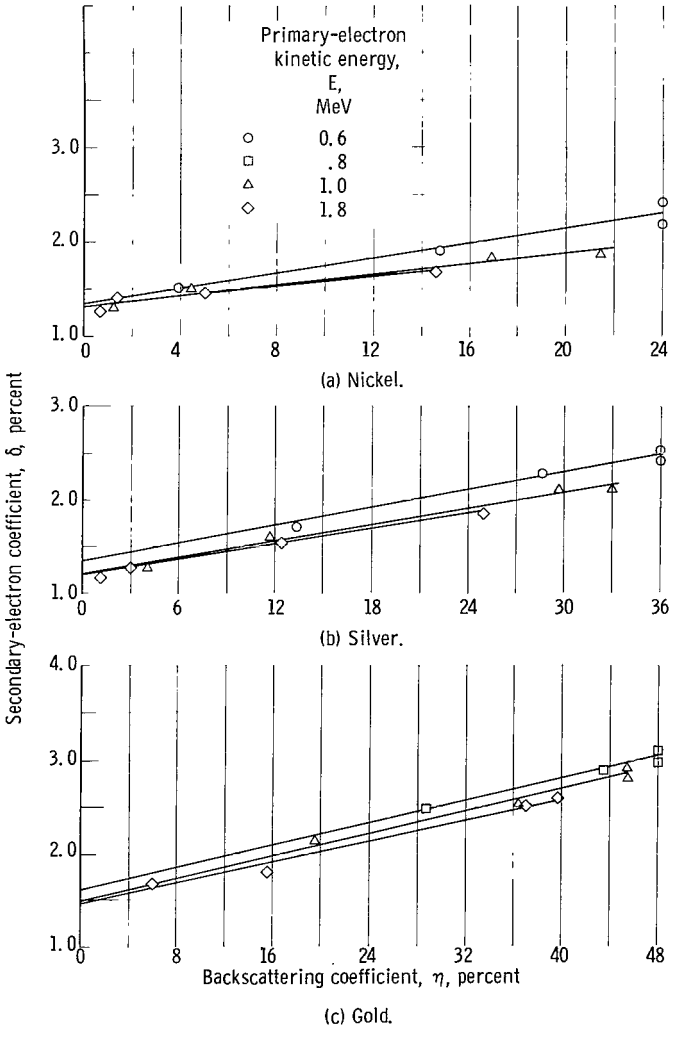

Figure 11. - Secondary-electron coefficient as function of backscattering coefficient for normal incidence for nickel, silver, and gold .

The secondary yields for the different targets of the same metal with the same backscattering yield differ by up to 12 percent because of differences in surface condition.

Secondary yield as function of backscattering yield. - It is clear from figure 9 that the secondary yield increases as the target thickness (and thus backscattering) increases, except where surface effects mask the trend.

With the assumption that β, the efficiency of backscattered electrons in producing secondaries, is independent of target thickness, equation (11) predicts that this increase should be linear with the backscattering coefficient. Cross plots of the total secondary coefficient against the backscattering coefficient were made, but, for some metals, variations in the secondary yield (due presumably to changes in surface condition) prevented determining whether or not the increase was linear. A definite linear increase was observed, however, for nickel, silver, and gold, as shown in figure 11. Values for the parameters of equation (11) (β and δ_p^o), as determined from the slopes

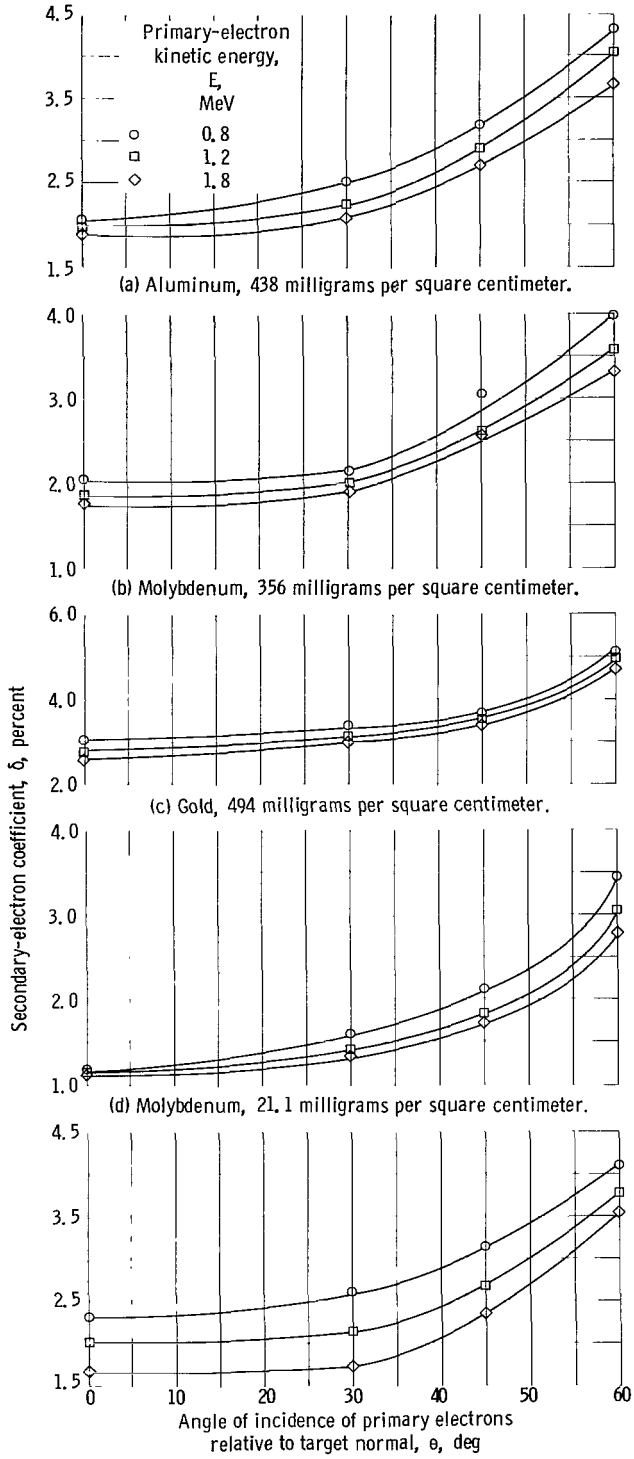

Figure 12. - Secondary-electron coefficient as function of angle of incidence of primary electrons relative to target normal for aluminum, molybdenum, and gold targets.

and intercepts of the lines in figure 11, are shown in the following table.

Target metal	Primary-electron kinetic energy, E, MeV	Secondary-electron coefficient due to primaries, δ_p^o, percent	Efficiency of the backscattered electrons for forming secondary electrons, β, percent
Nickel	0.6	1.4	2.9
	1.0	1.3	2.2
	1.8	1.3	1.9
Silver	0.6	1.4	2.3
	1.0	1.2	2.4
	1.8	1.2	2.2
Gold	0.8	1.6	1.[illegible]
	1.0	1.5	2.0
	1.8	1.5	1.9

The values for the yield of secondaries due to normally incident primaries of 1.3 and 1.4 percent at 1.0 and 0.6 MeV for nickel are in general agreement with reference 6, but about 10 percent lower in absolute value. These yields do not change much with energy, in accord with equations (9) and (10).

The values of β obtained also show little dependence on energy between 0.6 and 1.8 MeV. The magnitudes are between 1.8 and 2.9. For incident electrons with energies of 2 keV, much larger values of β have been measured (7.1 for nickel, 7.9 for silver, and 9.3 for gold, refs. 15 and 16). The explanation for this difference is that the average energy of the backscattered electrons passing through the secondary-electron escape zone is a larger fraction of the incident electron energy for 0.6-MeV electrons than for low keV electrons (ref. 17, p. 355). Since energy loss of an electron in the 1-keV to 0.6-MeV

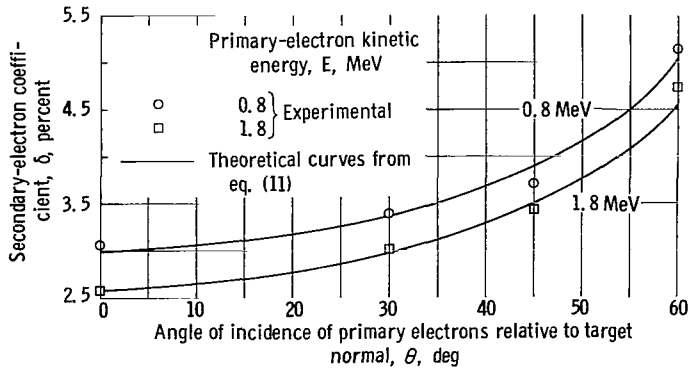

Figure 13. - Comparison of theoretical curves and experimental data. Secondary-electron coefficient as function of angle of incidence of primary electrons relative to target normal for 494-milligram-per-square-centimeter gold target.

energy range is smaller the higher its energy (eq. (10)), less energy is deposited in the escape zone, and fewer secondaries are excited for the higher energy primary electrons.

Secondary-electron coefficient as function of angle of incidence. - The experimental values for total secondary yield are plotted against the angle of incidence of the primary electrons in figure 12 for the same targets as those discussed in the section "Backscattering as function of angle of incidence." Primary-electron energies of 0.8, 1.2, and 1.8 MeV are used.

For all five targets, the total secondary coefficient increases as the angle of incidence of the primary electrons increases. The highest value measured is for gold at the largest angle, 60°, and the lowest energy, 0.8 MeV, where the secondary yield equals 5.2 percent.

A curve of total secondary yield as a function of angle of incidence θ, as equation (11) shows, is a composite of the $\sec \theta$ dependence of the secondary yield due to primaries (eq. (9)) and the variation of backscattering yield as a function of angle of incidence for the particular target. Percentagewise, the total secondary yield rises faster with the angle of incidence for aluminum and for thin molybdenum than it does for the other targets (see figs. 12(a) and (d)). This effect is due to the backscattering yield rising rapidly with the angle of incidence for these targets (see figs. 7(a) and (d), p. 15).

Curves of total secondary yield as a function of angle of incidence for gold can be computed from equation (11) by using the measured yields of secondaries due to primaries at normal incidence and the normal incidence efficiencies of backscattered electrons for producing secondaries. The curves are in reasonable agreement with the experimental points, as shown in figure 13. This indicates that β is not strongly dependent on the angle of incidence between 0° and 60°.

CONCLUDING REMARKS

An investigation was undertaken to determine the backscattering and secondary-electron yield from metal targets of various thicknesses. The targets were bombarded at different angles of incidence with electrons having an energy range of 0.6 to 1.8 MeV. Backscattering and secondary-electron coefficients were presented in graphical form as a function of primary energy, primary angle of incidence, target material, and target thickness. Backscattering coefficients were measured as low as 0.4 percent and as high as 62 percent, and

secondary-electron yields ranged from 1.1 to 5.2 percent.

It was found that the variation of backscattering coefficient with target thickness could be correlated, for each material, by plotting the ratio of the coefficient to its value for infinite thickness against the ratio $2t/R$, where t is thickness and R is range of the primary electrons in the material.

Except for variations due to surface effects, the secondary coefficient at normal incidence increased linearly with the backscattering coefficient, as had been observed at keV energies. For nickel, silver, and gold the backscattered electrons produced secondary electrons with approximately twice the efficiency of the primary electrons.

Backscattering yields were found to increase with increasing thickness and atomic number. Large angles of incidence tended to increase backscattering for all materials and thicknesses. In general, the coefficient of backscattering, in the energy range of interest, is larger than the secondary-electron coefficient.

With the data obtained in this and previous investigations, it is possible to estimate the effect of backscattering and secondary emission on the performance of the beta radioisotope cell. These estimates, together with empirical formulas for representing the backscattering data are the subjects of a current investigation.

Lewis Research Center,
National Aeronautics and Space Administration,
Cleveland, Ohio, January 19, 1965.

APPENDIX A

SYMBOLS

A	atomic weight
B_i	fraction of twice-backscattered electrons emitted in hemisphere containing beam hole
c	velocity of light
E	primary-electron kinetic energy
E'	primary-electron total energy, $E + m_o c^2$
e	electron charge
I	ionization constant in energy loss rate formula
I_{col}	current to collecting electrodes
I_{col}^{+}	current to collecting electrodes with $V_T - V_S = 122$ volts
I_{col}^{-}	current to collecting electrodes with $V_T - V_S = -30$ volts
I_F	Faraday cup and target current
I_i	incident beam current
K	constant
m_o	electron rest mass
N	number of atoms per unit volume in stopping material
P_{B_i}	probability of escape for electrons emitted in hemisphere containing beam hole
P_{T_i}	probability of escape for electrons emitted in hemisphere containing Faraday cup and target
R	range of electron
T_i	fraction of twice-backscattered electrons emitted in hemisphere containing Faraday cup and target
t	target thickness, mg/sq cm
V_S	screen voltage

V_T target voltage

v particle velocity

W number of once-backscattered electrons

W_i number of once-backscattered electrons falling between α_i and α_{i-1}

W_L number of twice-backscattered electrons not recollected

x linear distance

y effective secondary-electron production depth

Z atomic number

α angle with target normal

α_i ith angle with target normal

β efficiency of the backscattered electrons for forming secondary electrons

Δ backdirected electron yield

δ secondary-electron coefficient

δ_P secondary-electron coefficient due to primaries

δ_P^o secondary-electron coefficient due to primaries at $\theta = 0^o$

ϵ secondary-electron constant characteristic of the material

η backscattering coefficient

η_i backscattering coefficient for aluminum at ith angle

η_{max} backscattering coefficient for infinite thickness

θ angle of incidence of primary electrons relative to target normal

θ' scattering angle for single scattering

σ Rutherford scattering cross section

Φ angle between projection of path from target to collector in x',y'-plane and x'-axis

Ω solid angle into which electrons are backscattered

APPENDIX B

BACKSCATTERING CURRENT FROM COLLECTING ELECTRODES

Twice-backscattered electrons, which come off of the collecting electrodes and are not recollected but instead hit the target and Faraday cup or escape, cause an error in the measured values of η. The geometry of the target-collector arrangement makes it necessary to estimate the current numerically.

For bombardment at normal incidence, the once-backscattered electrons are assumed to come off of the target in a cosine distribution:

$$\frac{dW(\alpha)}{d\Omega} = K \cos \alpha \tag{B1}$$

where dW is the differential of the number of once-backscattered electrons, α is the angle between the target normal and the path of the once-backscattered electrons, $d\Omega$ is the differential of the solid angle into which the electrons are backscattered, and K is a constant.

The collector is a modified cone. The effect of the screen is replaced by the effect of the collector area which is shielded by the screen. For the calculation, the collector area is divided into seven rings by the choice of eight angles with the target normal, which are denoted by α_i (see fig. 14). The number of once-backscattered electrons W_i which fall between the angles α_i and α_{i-1} divided by the total number of backscattered electrons W is from equation (B1):

$$\frac{W_i}{W} = \frac{K \int_0^{2\pi} \int_{\alpha_{i-1}}^{\alpha_i} \cos \alpha \sin \alpha \, d\alpha \, d\Phi}{K \int_0^{2\pi} \int_0^{\pi/2} \cos \alpha \sin \alpha \, d\alpha \, d\Phi} \tag{B2}$$

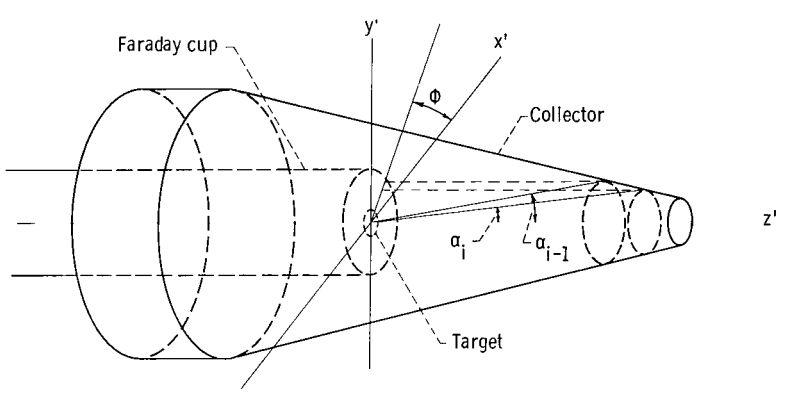

Figure 14. - Division of collector area into rings for calculation of number of twice-backscattered electrons.

where Φ is the angle between the projection of the path from target to collector in the x',y'-plane and the x'-axis. The integration results in

$$\frac{W_i}{W} = \sin^2\alpha_i - \sin^2\alpha_{i-1} \tag{B3}$$

For each ring of collector area, the ratio of twice-backscattered electrons to the total number of once-backscattered electrons from the target is obtained by measuring the angle between the normal to the collector and the average path from target to collector, reading off for this angle the backscattering coefficient for thick aluminum η_i from figure 7(a) (p. 15) and multiplying W_i/W by this η_i. In the actual case, the once-backscattered electrons had a distribution of energies. All the once-backscattered electrons were taken to have an energy of 0.8 MeV in choosing the η_i.

The twice-backscattered electrons which are not recollected W_L are found by dividing the collector backscattered electrons into two groups. One group is the fraction emitted in the hemisphere containing the beam hole B_i, and the other group is the fraction emitted in the hemisphere toward the target and Faraday cup T_i. The probabilities of escape (P_{B_i} and P_{T_i}) are estimated for each group as a whole. Then W_L is the sum

$$W_L = \sum_{i=1}^{7} \frac{W_i}{W} \eta_i \left(B_i P_{B_i} + T_i P_{T_i}\right) \tag{B4}$$

The fractions B_i and T_i are estimated by using data from reference 7 on the angular distribution in the plane of the incident beam and the target normal of the backscattered electrons. It is assumed that the distribution does not change much with changes in the energy of the primary electrons and that the distribution is representative of that in other planes. Upper limits are used for the probabilities P_{B_i} and P_{T_i}. The values are computed as the ratio of the area of the spherical segment involved to the area of a hemisphere, wherein the radii are from points on the z'-axis opposite the points on the collector. When the calculations are made and the sum is taken, the estimate is that less than 5.2 percent of the once-backscattered electrons are lost because of a second backscatter from the collector.

REFERENCES

1. Low, Charles A., Jr.; and Mickelsen, William R.: An Electrostatic Propulsion System with a Direct Nuclear Electrogenerator. Paper Presented at IAS Nat. Prop. Meeting, Cleveland (Ohio), Mar. 9, 1962. (See also Aerospace Eng., vol. 21, no. 12, Dec. 1962, pp. 58-59; 72-87.)

2. Dekker, J. J.: Secondary Electron Emission. Solid State Physics, Advances in Res. and Applications, Vol. 6, Academic Press, Inc., 1958, pp. 251-311.

3. Kollath, R.: Sekundarelectronen-Emissionfeste Korper bei Bestrahlung mit Elektronen. Handbuch der Physik, S. Flugge, ed., Bd. 21, Springer-Verlag (Berlin), pp. 233-303.

4. Wright, Kenneth, A.; and Trump, John G.: Back-Scattering of Megavolt Electrons from Thick Targets. J. Appl. Phys., vol. 33, no. 2, Feb. 1962, pp. 687-690.

5. Trump, John G.; and van de Graaff, R. J.: The Insulation of High Voltages in Vacuum. J. Appl. Phys., vol. 18, no. 3, Mar. 1947, pp. 327-332.

6. Schultz, Arvid A.; and Pomerantz, Martin A.: Secondary Electron Emission Produced by Relativistic Primary Electrons. Phys. Rev., vol. 130, no. 6, June 1963, pp. 2135-2141.

7. Frank, H.: Zur Vielfachstreuung und Rückdiffusion schneller Elektronen nach Durchgang durch dicke Schichten. Z. Naturforsch., bd. 14a, no. 3, Mar. 1959, pp. 247-261.

8. Cleland, M. R.; and Morganstern, K. H.: A New High-Power Electron Accelerator. IRE Trans. on Industrial Electronics, vol. IE-7, no. 2, July 1960, pp. 36-40.

9. Evans, Robley D.: The Atomic Nucleus. McGraw-Hill Book Co., Inc., 1955.

10. Snyder, H. S.; and Scott, W. T.: Multiple Scattering of Fast Charged Particles. Phys. Rev., vol. 76, no. 2, July 1949, pp. 220-225.

11. Katz, L.; and Penfold, A. S.: Range-Energy for Electrons and the Determination of Beta-Ray End-Point Energies by Absorption. Rev. Mod. Phys., vol. 24, no. 1, Jan. 1952, pp. 28-44.

12. Glendenin, Lawrence E.: Determination of the Energy of Beta Particles and Photons by Absorption. Nucleonics, vol. 2, Jan. 1948, pp. 12-32.

13. Kanter, H.: Contribution of Backscattered Electrons to Secondary Electron Formation. Phys. Rev., vol. 121, no. 3, Feb. 1, 1961, pp. 681-684.

14. Kanter H.: Energy Dissipation and Secondary Electron Emission in Solids. Phys. Rev., vol. 121, no. 3, Feb. 1, 1961, pp. 677-681.

15. Bronshtein, I. M.; and Fraiman, B. S.: Secondary Emission Properties of Metals and Semiconductors and the Periodic System of Elements. Soviet Phys. - Solid State, vol. 3, no. 10, Apr. 1962, pp. 2337-2339. (Trans. from Fiz. Tverd. Tela, vol. 3, no. 10, Oct. 1961, pp. 3220-3223.)

16. Bronshtein, I. M.; and Segal, R. B.: Inelastic Scattering of Electrons and Secondary-Electron Emission in Certain Metals. II. Soviet Phys. - Solid State, vol. 1, no. 10, Apr. 1960, pp. 1375-1382. (Trans. from Fiz. Tverd. Tela, vol. 1, no. 10, Oct. 1959, pp. 1500-1508.)

17. Sternglass, Ernest J.: Backscattering of Kilovolt Electrons from Solids. Phys. Rev., vol. 95, no. 2, July 15, 1954, pp. 345-358.

TABLE I. - BACKSCATTERING COEFFICIENT

Target metal	Target thickness, t, mg/sq cm	Primary-electron kinetic energy, E, meV						
		0.6	0.8	1.0	1.2	1.4	1.6	1.8
		Backscattering coefficient, η						
Aluminum	12.7	0.0071	0.0059	0.0049	0.0044	0.0042	0.0040	0.0039
	59.4	.071	.035	.019	.014	.010	.0090	.0077
	90.0	.096	.066	.037	.025	.017	.013	.011
	438.3	[a].104	[a].097	[a].088	[a].082	[a].076	[a].071	[a].065
Iron	19.0	0.027	0.013	0.0080	0.0062	0.0050	0.0044	0.0040
	41.7	.115	.058	.030	.020	.015	.012	.010
	100.5	.217	.180	.122	.086	.058	.042	.030
	259.4	[a].219	[a].208	[a].195	[a].185	.170	.153	.131
Nickel	20.5	0.039	0.020	0.012	0.010	0.0080	0.0074	0.0070
	47.2	.146	.082	.044	.029	.020	.016	.013
	118.8	.239	.216	.169	.126	.093	.070	.050
	250.9	[a].238	[a].226	[a].213	[a].202	.187	.169	.145
Molybdenum	21.1	0.069	0.035	0.020	0.015	0.012	0.010	0.0090
	150.4	.328	.313	.282	.244	.199	.163	.130
	253.7	.328	.313	.300	.286	.270	.246	.222
	356.0	[a].328	[a].314	[a].300	[a].289	[a].277	.266	.252
Silver	28.2	0.134	0.072	0.039	0.027	0.019	0.015	0.013
	54.6	.286	.197	.119	.082	.056	.041	.030
	127.9	.357	.338	.295	.249	.199	.161	.125
	246.7	[a].357	[a].344	[a].328	[a].316	.298	.278	.251
Tantalum	43.4	0.355	0.223	0.150	0.106	0.080	0.060	0.045
	129.0	.461	.443	.401	.357	.298	.253	.208
	186.7	.460	.447	.428	.408	.372	.341	.299
	427.0	[a].460	.446	[a].430	[a].418	[a].404	[a].392	[a].378
Gold	48.3	0.392	0.288	0.195	0.145	0.102	0.079	0.059
	93.0	.478	.439	.362	.304	.241	.196	.156
	242.1	.483	.470	.454	.440	.422	.401	.370
	493.7	[a].487	[a].471	[a].455	[a].442	[a].427	[a].415	[a].401

[a]Backscattering coefficient for infinite thickness, η_{max}.

TABLE II. - TARGET THICKNESS AS FRACTION OF HALF-RANGE

Target metal	Target thickness, t, mg/sq cm	Primary-electron kinetic energy, E, MeV						
		0.6	0.8	1.0	1.2	1.4	1.6	1.8
		Target thickness/half-range						
Aluminum	12.7	0.121	0.082	0.062	0.049	0.041	0.035	0.030
	59.4	.564	.384	.288	.230	.189	.163	.142
	90.0	.855	.582	.437	.348	.288	.247	.215
	438.3	4.16	2.83	2.13	1.69	1.40	1.20	1.05
Iron	19.0	0.174	0.118	0.089	0.071	0.058	0.050	0.044
	41.7	.382	.260	.195	.156	.129	.110	.096
	100.5	.920	.627	.470	.374	.310	.265	.231
	259.4	2.38	1.62	1.21	.967	.802	.686	.597
Nickel	20.5	0.192	0.131	0.098	0.078	0.065	0.055	0.048
	47.2	.442	.301	.226	.180	.148	.128	.111
	118.8	1.11	.758	.569	.453	.374	.321	.279
	250.9	2.35	1.60	1.20	.957	.790	.678	.590
Molybdenum	21.1	0.182	0.124	0.093	0.074	0.061	0.053	0.046
	150.4	1.30	.840	.664	.529	.437	.375	.326
	253.7	2.19	1.49	1.12	.892	.737	.632	.550
	356.0	3.07	2.09	1.57	1.25	1.03	.886	.772
Silver	28.2	0.242	0.165	0.124	0.098	0.081	0.070	0.063
	54.6	.468	.319	.240	.190	.158	.135	.118
	127.9	1.09	.748	.561	.447	.370	.316	.276
	246.7	2.12	1.44	1.08	.862	.713	.611	.532
Tantalum	43.4	0.345	0.235	0.177	0.140	0.116	0.100	0.087
	129.0	1.02	.700	.525	.418	.345	.296	.258
	186.7	1.49	1.01	.760	.605	.500	.429	.373
	427.0	3.40	2.32	1.74	1.38	1.14	.981	.854
Gold	48.3	0.382	0.260	0.195	0.155	0.129	0.110	0.095
	93.0	.736	.502	.376	.300	.248	.212	.184
	242.1	1.92	1.30	.979	.780	.644	.552	.481
	493.7	3.91	2.66	1.99	1.59	1.31	1.13	.982

2122185
02

"The aeronautical and space activities of the United States shall be conducted so as to contribute . . . to the expansion of human knowledge of phenomena in the atmosphere and space. The Administration shall provide for the widest practicable and appropriate dissemination of information concerning its activities and the results thereof."

—NATIONAL AERONAUTICS AND SPACE ACT OF 1958

NASA SCIENTIFIC AND TECHNICAL PUBLICATIONS

TECHNICAL REPORTS: Scientific and technical information considered important, complete, and a lasting contribution to existing knowledge.

TECHNICAL NOTES: Information less broad in scope but nevertheless of importance as a contribution to existing knowledge.

TECHNICAL MEMORANDUMS: Information receiving limited distribution because of preliminary data, security classification, or other reasons.

CONTRACTOR REPORTS: Technical information generated in connection with a NASA contract or grant and released under NASA auspices.

TECHNICAL TRANSLATIONS: Information published in a foreign language considered to merit NASA distribution in English.

TECHNICAL REPRINTS: Information derived from NASA activities and initially published in the form of journal articles.

SPECIAL PUBLICATIONS: Information derived from or of value to NASA activities but not necessarily reporting the results of individual NASA-programmed scientific efforts. Publications include conference proceedings, monographs, data compilations, handbooks, sourcebooks, and special bibliographies.

Details on the availability of these publications may be obtained from:

SCIENTIFIC AND TECHNICAL INFORMATION DIVISION

NATIONAL AERONAUTICS AND SPACE ADMINISTRATION

Washington, D.C. 20546